JOC The Journal of Organic Chemistry

Article

pubs.acs.org/joc

Mixed Phenyl and Thiophene Oligomers for Bridging Nitronyl Nitroxides

Kubandiran Kolanji,[†] Prince Ravat,[†,∥] Artem S. Bogomyakov,[‡] Victor I. Ovcharenko,[‡] Dieter Schollmeyer,[§] and Martin Baumgarten*[,†]

[†]Max Planck Institute for Polymer Research, Ackermannweg 10, 55128 Mainz, Germany

[‡]International Tomography Center, Siberian Branch, Russian Academy of Sciences, Institutskaya Str. 3a, 630090 Novosibirsk, Russian Federation

[§]Institut fuer Organische Chemie, Universitaet Mainz, Duesbergweg 10-14, 55099, Mainz, Germany

Supporting Information

ABSTRACT: The synthesis of four nitronyl nitroxide (NN) biradicals is described which are conjugatively linked through *p-ter*-phenyl (PPP), *ter*-thiophene (TTT) and alternating phenylene (P) and thiophene (T) units as PTP and TPT. We first utilized Suzuki and Stille coupling reactions through protection and deprotection protocols to synthesize these (NN) biradicals. Single crystals were efficiently grown for radical precursors of **3**, **5**, **6**, **PPP-NNSi**, **PTP-NNSi**, and final biradicals of **TTT-NN**, **TPT-NN**, and **PPP-NN**, whose structures and molecular packing were examined by X-ray diffraction studies. As a result, much smaller torsions between the NN and thiophene units (∼10°) in **TTT-NN** and **TPT-NN** than for NN and phenyl units (∼29°) in **PPP-NN** were observed due to smaller hindrance for a five vs a six membered ring. All four biradicals **TTT-NN**, **TPT-NN**, **PTP-NN**, and **PPP-NN** were investigated by EPR and optical spectroscopy combined with DFT calculations. The magnetic susceptibility was studied by SQUID measurements for **TTT-NN** and **TPT-NN**. The intramolecular exchange interactions for **TPT-NN** and **TTT-NN** were found in good agreement with the ones calculated by broken symmetry DFT calculations.

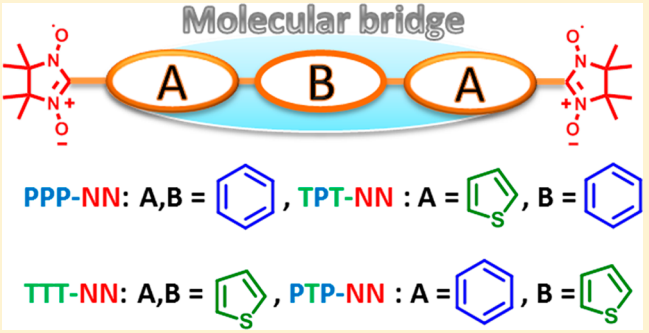

INTRODUCTION

Organic molecules are currently of high impact in the field of materials science owing to the low cost of fabrication and the simplicity and flexibility of the device.[1−3] Stable radical moieties connected with aromatic oligomers have generated great attention[4,5] due to their potential applications in spintronics,[6−8] quantum molecular magnets,[9,10] spin-labeling,[11] spin-trapping,[12] magneto conducting materials,[13−15] magnetic resonance imaging,[16] biomedicine,[17] organic photo excited spin systems,[18,19] field effect transistors,[20−22] solar cell,[23−26] sensors,[27] and batteries.[28,29] All of these properties are dependent on the type of radical entities and their connection to a conjugated core.

The spin−spin interaction between the stable free radicals such as nitronylnitroxides (NN), *tert*-butylnitroxides, iminonitroxides (IN), and verdazyl (VZ) can be fine-tuned through their combination with conjugated oligomers.[30−41] Previously reported NN biradicals were built upon biphenyl,[42] terpyridine,[43] pyrene,[44] and tolane[45] as a π-bridge, and their optical, electrochemical, EPR, and magnetic properties were studied.

Weakly antiferromagnetically (AFM) coupled spin-dimers with singlet ground state which can be tuned by a magnetic field to the triplet state are of particular interest.[46] The self-assembly of the spin-dimer molecules is used for the development of solid state Bose−Einstein condensation (BEC) materials,[47−49] where two guiding principles should hold: (1) The intramolecular exchange coupling should dominate and exceed the intermolecular coupling, and (2) the intramolecular coupling should be small enough for laboratory-scaled magnets to switch the spin state (ground state singlet into the triplet state).

Recently, we found that tolane bridged NN biradicals undergo quasi two-dimensional magnetic field induced quantum phase transition at very low temperatures in the routine laboratory magnetic field up to 11 T[41]. While thiophene extension with NN biradical entities were explored,[50,51] mixed thiophene and phenylene oligomers with NN radicals are not reported to the best of our knowledge to tune the magnetic and electronic properties of biradical systems. From previous observations, the intramolecular magnetic interactions depend on the conjugation among the aromatic cores, the distance between the radicals, and the torsional angles among NN and the aromatic bridge.

Received: March 8, 2017
Published: June 30, 2017

DOI: 10.1021/acs.joc.7b00435
J. Org. Chem. 2017, 82, 7764−7773

Therefore, it is necessary to better understand the effect of the aromatic bridge on the spin−spin interaction between the radical units. Hence, we designed four molecular bridges, *p-ter*-phenyl, (PPP), *ter*-thiophene, (TTT), and two mixed thiophene and phenylene oligomers (TPT and PTP) (Figure 1) and investigated the molecular length and torsion angles

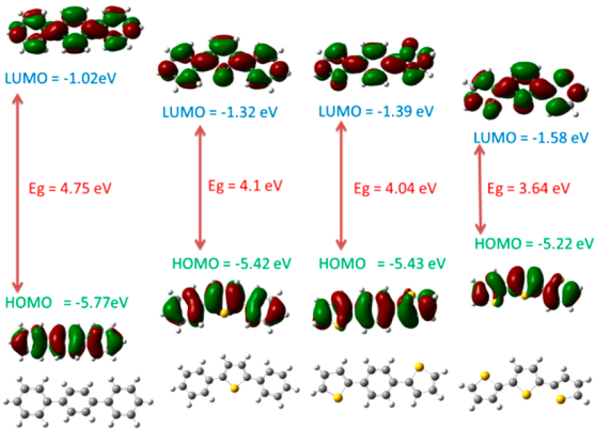

Figure 1. Optimized structure of **PPP**, **PTP**, **TPT**, and **TTT** by using the B3LYP functional and 6-31G(d) basis set and HOMO, LUMO, and energy gap (Eg) of the bridging oligomers.

(Figure S1), as well as their HOMO, LUMO, electron density distribution, and the energy gap (E_g) by density functional theory (DFT). The E_g of TTT is 3.64 eV, which is much lower than that for PPP (4.75 eV), TPT (4.10 eV), and PTP (4.04 eV). On the basis of these π-units (PPP, TTT, TPT, and PTP), four (NN) biradicals (**TPT-NN**, **PPP-NN**, **TTT-NN**, and **PTP-NN**) were designed (Figure 2). The NN radical units are

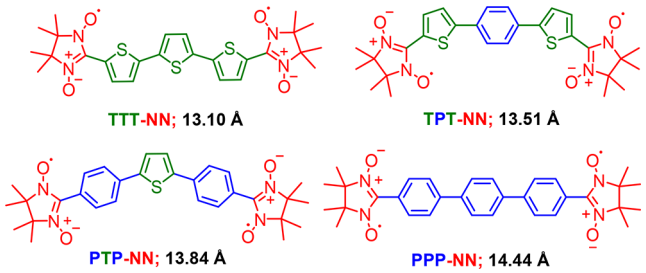

Figure 2. Structures of **TTT-NN**, **TPT-NN**, **PTP-NN**, and **PPP-NN**; distance between C2−C2 of NN.

attached to the para-substitution of the phenyl unit for **PPP-NN** and **PTP-NN**, and the NNs are attached to the fifth-position of the thiophene ring for **TTT-NN** and **TPT-NN**. In the molecular design, we predicted by spin polarization rule that the spins on the NN groups are AFM coupled to each other (Figure S2).

Hence, as a model system for BEC in the solid state, our aim is to synthesize weakly AFM coupled biradicals, where the intramolecular exchange interaction can be controlled or adjusted in the range of J/k_B = 2−10 K. These biradicals were characterized by EPR, UV−vis spectrometry, and single crystal X-ray structural analysis, and their magnetic properties were investigated by SQUID magnetometry and supported with the quantum chemical DFT calculations.

RESULTS AND DISCUSSION

Synthesis of Biradicals. The *tert*-butyldimethylsilyl (TBDMS) protected bromothiophene monoradical moiety **3** was introduced by Suzuki coupling reaction with 1,4-benzenediboronic acid bis(pinacol) ester and deprotection to obtain **TPT-NN** (Scheme 1). This was necessary since the first attempt to synthesize the target compound **TPT-NN** by condensation of dialdehydes with 2,3-bis(hydroxyamino)-2,3-dimethylbutane (BHA) failed Scheme S1, although it is often announced in the literature as a suitable step. **PPP-NN** was synthesized from dialdehydes with low (5.2%) yield.[52] This was mainly because of the poor solubility of the corresponding dialdehyde precursor in common organic solvents. Later, a similar synthetic protocol was applied to synthesize the other three biradicals. Reaction of the 5-bromo-2-thiophenecarboxaldehyde or 4-bromobenzaldehyde with BHA at room temperature in methanol yielded compounds **2** and **4** with good yields (>80%). Then, the N−OH groups were protected with TBDMS by *tert*-butyldimethylsilyl chloride (*t*-BuMe_2SiCl) in the presence of imidazole in DMF as solvent to afford **3** and **5** with excellent yields (>90%). The highly stable biradical precursors **TPT-NNSi** and **PPP-NNSi** were obtained by Suzuki coupling reactions between **3** or **5** with 1,4-benzenediboronic acid bis(pinacol) ester in moderate to good (>60%) yield.

The preparation of **PTP-NNSi** from **5** either by Suzuki coupling between **5** and thiophene-2,5-diboronic- bis(pinacol) ester (**7**) or by Stille coupling between **5** with 2,5-bis(trimethylstannyl)thiophene (**8**) was unsuccessful. Therefore, boronic-bis(pinacol)ester (**6**) was prepared from **5** by its treatment with *n*-BuLi, followed by 2-isopropylboronic acid and pinacol ester. The Suzuki coupling of 2,5-dibromothiophene and **6** successfully yielded **PTP-NNSi** in 66% yield. An attempt to synthesize **TTT-NNSi** by Suzuki coupling with **3** and thiophene-2,5-diboronic-bis(pinacol)ester provided only 18% along with 51% of the monosubstituted side product obtained. The yield of **TTT-NNSi** could be highly improved by a Stille coupling reaction between **3** and 2,5-bis(trimethylstannyl)-thiophene (74%). All the precursors were characterized by NMR and mass spectra, and the precursors **3**, **5**, **6**, **PPP-NNSi**, and **PTP-NNSi** were also verified by single crystal X-ray structure analysis (Figures S3−S7).

All biradicals **TTT-NN**, **TPT-NN**, **PTP-NN**, and **PPP-NN** were obtained by subsequent cleavages of the (TBDMS) protecting groups in one step with tetrabutylammonium fluoride (TBAF) in THF (Scheme 1, bottom). The reaction was carefully monitored by TLC to get the best yield of NN biradicals, which were purified by column chromatography. These biradicals were characterized by EPR and UV−vis spectroscopy and ESI mass spectrometry. The structures of **TTT-NN**, **TPT-NN**, and **PPP-NN** were further verified by single crystal X-ray analysis (Figures S8−S10).

Optical Properties. The UV−vis absorption spectra of the biradicals (**TTT-NN**, **TPT-NN**, **PTP-NN**, and **PPP-NN**) were measured in toluene ($c \sim 10^{-5}$ M) at room temperature and are depicted in Figure 3. The absorption data of biradicals (λ_{max}, ε, and optical gap E_g) are given in Table 1. The absorption spectra of the biradicals are compared with their precursors (Figure S12) together with their data summarized in Table S2. Only one absorption band was observed for all precursors (**TPT-NNSi**, **PPP-NNSi**, **PTP-NNSi**, and **TTT-NNSi**) due to the $\pi-\pi^*$ transition of the π-bridge. All four biradicals exhibited two absorption bands, around 280−500 nm due to the $\pi-\pi^*$

DOI: 10.1021/acs.joc.7b00435
J. Org. Chem. 2017, 82, 7764−7773

Scheme 1. Synthetic Route of Biradicals

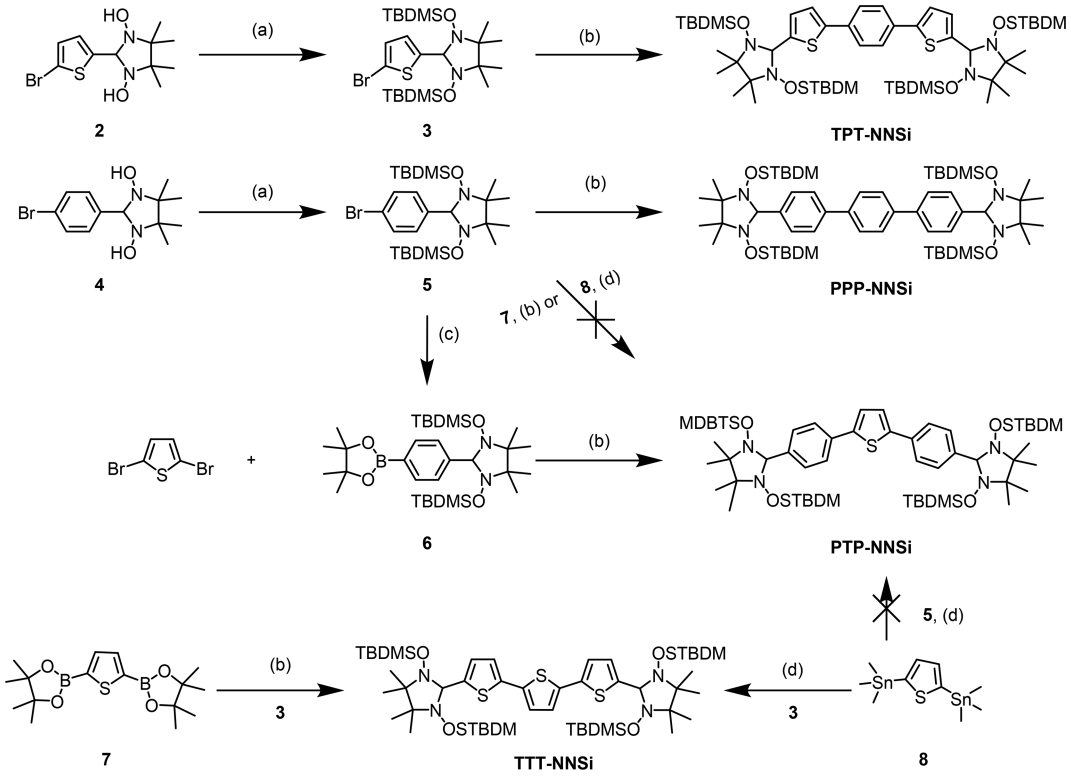

Reaction conditions: (a) *t*-BuMe$_2$SiCl, imidazole, DMF, 50 °C, (b) 1,4-benzenediboronic acid bis(pinacol) ester, K_2CO_3, Pd(PPh$_3$)$_4$, THF: H_2O, 60 °C (c) THF, -78 °C, *n*-BuLi, 2-isopropylboronic acid, pinacol ester, (d) Pd(PPh$_3$)$_4$, toluene:DMF, 60 °C.

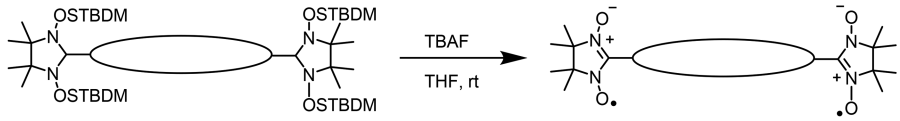

TPT-NNSi, PPP-NNSi, PTP-NNSi and **TTT-NNSi** **TPT-NN, PPP-NN, PTP-NN** and **TTT-NN**

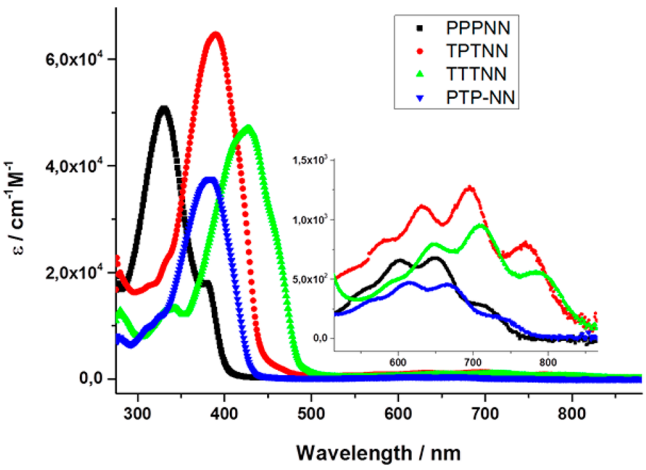

Figure 3. UV−vis absorption spectra of **PPP-NN**, **PTP-NN**, **TPT-NN**, and **TTT-NN** (~10^{-5} M in toluene).

transition of the conjugated backbone, and the characteristic $n-\pi^*$ transition of the NN radical moieties around 510−840 nm. The UV−vis spectra clearly indicate the presence of pure NN biradicals, without contamination by imino-nitroxide.

Table 1. Optical and EPR properties of TTT-NN, TPT-NN, PPP-NN, and PTP-NN

radicals	λ_{max}(nm), (ε cm^{-1} M^{-1})	E_g^{OP}[a]	$a_{N/2}$/mT[b]	g[b]
TTT-NN	427 (47315), 709 (956)	1.46	0.375	2.0067
TPT-NN	390 (64795), 695 (1267)	1.45	0.370	2.0065
PTP-NN	384 (37885), 669 (468)	1.63	0.381	2.0065
PPP-NN	331 (50757), 651 (680)	1.64	0.371	2.0066

[a]Optical energy gap calculated according to the absorption edge. [b]Calculated from EPR spectra.

The effect of the π-bridge on the absorption spectra for NN biradicals were investigated previously.[53] The $\pi-\pi^*$ transitions of the radicals are red-shifted compared to their protected precursors by 40−50 nm demonstrating the conjugation enhancement upon radical formation (Figure S12). Differences between the $n-\pi^*$ transitions can be traced back to better conjugation between a thiophene unit with NN than a phenylene with an NN unit (larger torsion).

DOI: 10.1021/acs.joc.7b00435
J. Org. Chem. 2017, 82, 7764−7773

The optical gaps E_g derived from the onset of the absorption edge of the $n-\pi^*$ transition for **TPT-NN** and **TTT-NN** are 1.45 and 1.46 eV, which are smaller than those for **PPP-NN** (1.64 eV) and **PTP-NN** (1.63 eV), respectively. The optical properties are thus tuned by enhancing the number and position of thiophenes in the molecular bridge.

EPR Studies. EPR spectra of all four biradicals were recorded in argon saturated toluene solutions. The room temperature, simulated and variable temperatures, and EPR spectra of **TPT-NN** are displayed in Figure 4. The EPR spectra

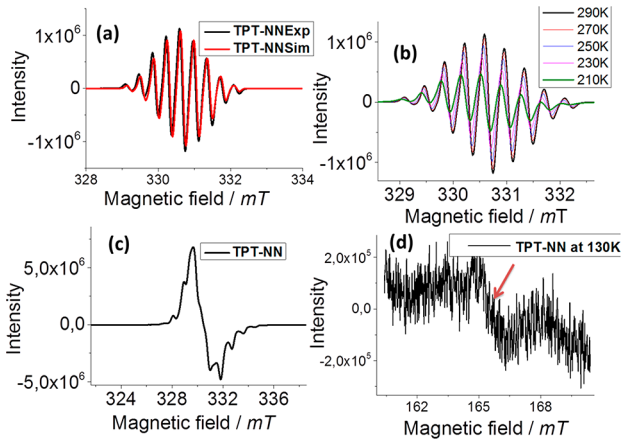

Figure 4. EPR spectra of the biradical **TPT-NN** in toluene ($\sim 10^{-4}$ M in toluene). (a) Room temperature, experimental (black), and simulated (red), (b) variable temperature (290–210 K), (c) ΔM_S = 1 transition of **TPT-NN** (black) at 130 K, and (d) half field ΔM_S = 2 transition at 130 K.

for **TTT-NN**, **PPP-NN**, and **PTP-NN** are provided in Figure S13. At room temperature, all four biradicals exhibited nine line spectra due to effective through-bond coupling via spin-polarization effects of the nitronyl nitroxides, indicating that exchange interactions J are much larger than the hyperfine coupling constants ($J \gg a_N$). The calculated g factors and hyperfine coupling constants ($a_{N/2}$) for all biradicals are summarized in Table 1. These values are in agreement with those typically observed in the NN biradicals found in the literature.

Upon decreasing temperature, the EPR signal intensity of **TPT-NN** is reduced, but the spectral widths are slightly broadened. The other biradicals followed the same characteristics (Figure S14). The frozen solution spectra of **TPT-NN** recorded at 130 K (Figure 4c) are asymmetric, and an anisotropic component of the monoradical overlaps with the ΔM_S = 1 region giving the different number of the shoulders in the outermost region. We verified the anisotropic nature by comparison with the thiophene monoradical (**T-NN**) frozen solution spectra at 130 K demonstrated in Figure S15a. The frozen solution spectra of **TTT-NN** recorded at 130 K are displayed in Figure S15b. The half field ΔM_S = 2 transition, although weak due to small zero field splitting, is clear evidence for the biradical nature of **TPT-NN**.

Crystal Structure Analysis. The magnetic interactions highly depend on the geometry and packing of the molecules in the crystal lattice. Therefore, crystal structure analysis is a vital requirement to understand magnetic interactions operating in synthesized biradical systems. While the crystals suitable for single crystal X-ray analysis were obtained by slow evaporation of DCM solution of biradicals for the **TPT-NN** and **TTT-NN**, the same for the **PPP-NN** were grown by slow diffusion of hexane to its solution in DCM.

The green needle of **TPT-NN** crystallized in the monoclinic, $P21/c$ space group, which has an inversion center of $C2$ symmetry and thus is symmetric to the central phenyl ring (Figure 5a). There is an intramolecular contact between the

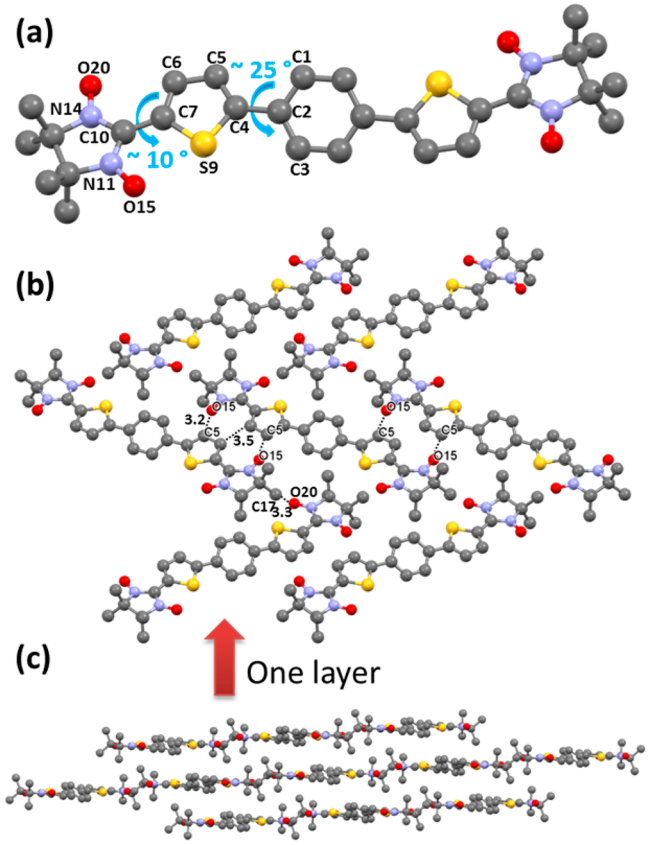

Figure 5. X-ray crystal structure of the **TPT-NN** (a) molecule, (b) edge-to-edge packing mode, and (c) face-to-face mode of crystal packing; hydrogen atoms are omitted for clarity.

thiophene sulfur (S) and the radical oxygen atom 2.85 Å (S9···O15), and the torsions between the radical moiety and thiophene unit are very small, only 9.5° (S9–C7–C10-N11) and 11.1° (C6–C7–C10–N14). The torsions between the central phenyl ring and the thiophene units, however, are larger with 25.7° for (C1–C2–C4–C5) and 24.2° for (C3–C2–C4–S9).

The molecular packing of the **TPT-NN** is displayed in Figure 5b, and the molecules are arranged in two different directions. The **TPT-NN** molecules are networking over the radical (N–O) unit through adjacent molecules of thiophene carbon as 3.2 Å for (O15–C5), and at the same time, the nearest molecule of N–O units also interacts with the first molecule of thiophene at 3.2 Å (C5–O15). The other side radical (N–O) units interact with the methyl group of nearest molecules at 3.3 Å (N–O20···C17), and methyl groups also interact with the next to the nearest molecule of N–O units. The $\pi-\pi$ distance between two **TPT-NNs** with the edge-to-edge (between thiophene and thiophene) approach of the molecules is 3.5 Å. The slipped π-stacked structures are shown in Figure 5c. A further examination of the crystal packing of the molecules showed that the molecules are stacked along the crystallographic a axis

DOI: 10.1021/acs.joc.7b00435
J. Org. Chem. 2017, 82, 7764–7773

in a face-to-face manner and that the $\pi-\pi$ distance is 3.63 Å for (C3···C10) as shown in Figure S11.

The green plate of **TTT-NN** crystallized in the monoclinic *P*21/n space group, and the X-ray single crystal structure is displayed in Figure 6a. The crystal data and refinement details

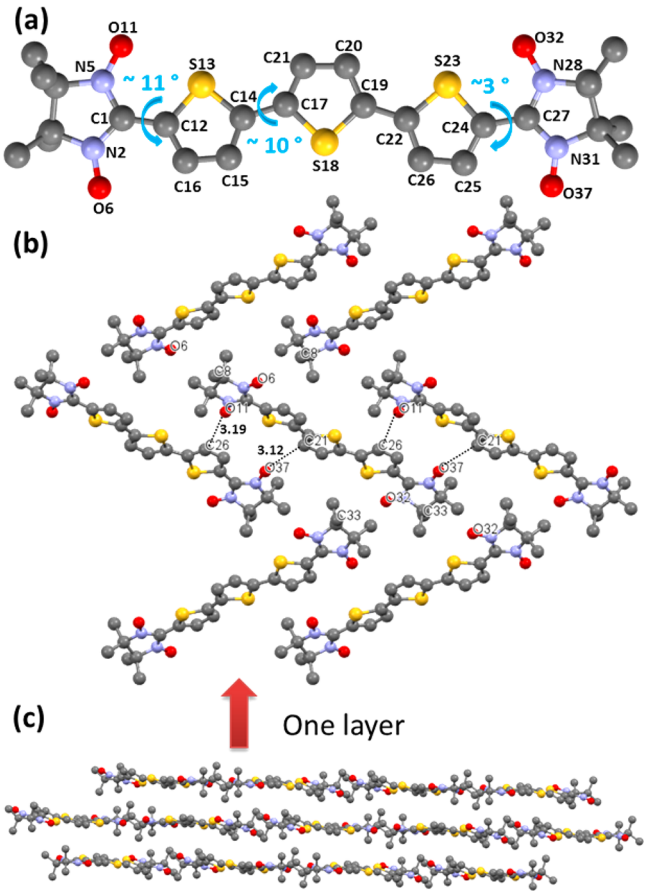

Figure 6. X-ray crystal structure of the **TTT-NN** (a) molecule, (b) crystal packing 2D mode, and (c) crystal packing 3D mode; hydrogen atoms are omitted for clarity.

are listed in Table 2. From the single crystal X-ray structure analysis, intramolecular contacts between radical N–O and sulfur atom of the thiophene are 2.9 Å for (O11–S13) and 2.8 Å for (S23–O32), respectively. Slightly different bond lengths are observed as well among thiophene and radical (NN) units which are 1.434 Å for (C1–C12) and 1.426 Å for (C24–C27) due to different modes of molecular packing.

The in-depth investigation of crystal packing of the **TTT-NN** shows that both the terminal thiophene and radical moiety (NN) are linked with different torsions which are 9.7° (N2–C1–C12–C16), 12.0° (N5–C1–C12–S13), 3.3° (S23–C24–C27–N28), and 3.2° (C25–C24–C27–N31). Also, all of the three thiophenes are connected with different torsions 10.6° (S13–C14–C17–C21), 11.1° (C15–C14–C17–S18), 7.3° (C20–C19–C22–S23), 9.1° (S18–C19–C22–C26). The molecular packing of the **TTT-NN** is given in the Figure 6b. Further analysis of molecular packing revealed that the molecules interact through the N–O unit with neighboring molecules of thiophene at 3.19 Å (O11–C26) at the same time as the second molecule N–O interacts with first molecule at 3.12 Å (C21–O37). The molecules are further stacked along

Table 2. Crystal Data and Structure Refinement Details of TPT-NN, TTT-NN, and PPP-NN

	TPTNN	TTTNN	PPP-NN
formula	$C_{28}H_{32}N_4O_4S_2$	$C_{26}H_{30}N_4O_4S_3$	$C_{32}H_{36}N_4O_4$
formula weight [g/mol]	552.20	558.74	540.65
crystal system	monoclinic	monoclinic	monoclinic
space group	*P*21/*c*	*P*21/*n*	*P*21/*n*
a (Å)	10.9341(19)	12.5445(12)	11.5064(9)
b (Å)	11.8693(18)	11.1792(7)	9.9143(10)
c (Å)	11.054(2)	20.4146(21)	12.9226(12)
β°	104.497(7)	107.466(8)	112.061(7)
Z	2	4	2
*wR*2	0.1100	0.2159	0.2959
*R*1	0.0776	0.0709	0.0963
density	1.322	1.359	1.314
μ (mm^{-1})	0.23	0.31	0.70
no. independent reflections	3331	6703	2446
no. of refined parameter	176	342	186
goodness of fit	1.140	1.013	0.961
CCDC	1501331	1501330	1501332

the crystallographic *b* axis (Figure S11). The $\pi-\pi$ distance between molecules is 3.58 Å for (N2–O6···C25).

The single crystal structure of **PPP-NN** is provided in Figure 7a, and crystallographic parameters are listed in Table 2. The

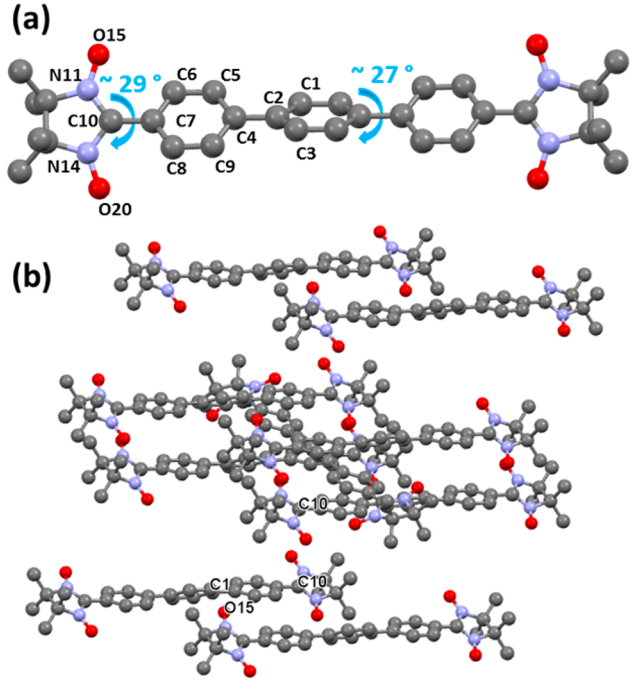

Figure 7. X-ray crystal structure of the **PPP-NN** (a) molecule and (b) crystal packing.

dark blue plate of **PPP-NN** crystallized in monoclinic, $P2_1/n$ space group and C_i symmetry. The radical NN units are connected with the phenyl ring with a torsion of 29.7° for (C6–C7–C10–N11) and 29.4° for C8–C7–C10–N14. The phenyl rings are linked with a torsion of 27.1° for (C1–C2–C4–C5) and 30.3° for (C3–C2–C4–C9). The molecular packing of the **PPP-NN** is shown in Figure 7b. The molecules

DOI: 10.1021/acs.joc.7b00435
J. Org. Chem. 2017, 82, 7764–7773

are extended through hydrogen bonding with adjacent molecules. There is no direct intermolecular π electron contact between molecules, but the intermolecular distance between molecules (edge to edge) is 3.42 Å for (N−O15···C1), and the face-to-face molecular distance is 4.66 Å for (C10−C10).

DFT Calculations. The DFT calculations (Gaussian 09 program package)[54] were carried out to find the influence of the π-bridge on the electronic properties and especially the intramolecular exchange interactions of the biradicals. The geometries were optimized by the UB3LYP/6-31G(d) level. The optimized structures of **PPP-NN**, **PTP-NN**, **TTT-NN**, and **TPT-NN** are shown in Figure S16.

The simplest Hamiltonian for the molecule with two exchange coupled unpaired electrons is given by $H = -2J_{12}S_1S_2$. The calculations were carried out by the broken-symmetry (BS) approach where the exchange interaction J becomes, $J/k_B = (E(BS) - E(T))/(S^2(T) - S^2(BS))$, with $E(BS)$ the energy of broken symmetry and $E(T)$ the triplet energy. S^2 are the eigenvalues of the spin operator, and for $S^2(BS)$ close to 1 and $S^2(T)$ close to 2 the direct exchange becomes $J/k_B = E(BS) - E(T)$. Thus, we applied the Heisenberg−Dirac−Van Vleck (HDVV) Hamiltonian.[55−59]

The UBLYP functional and 6-31G(d) basis set were used to elucidate J_{calc} from the optimized structure and compared with those from the X-ray structure of **TPT-NN**, **TTT-NN**, and **PPP-NN** (first two columns Table 3). The large deviation here

Table 3. Intra-dimer Magnetic Exchange Coupling Calculated, J_{calc}, and Experimental, J_{exp}, Values[a]

radicals	J_{calc} (K)[b]	J_{calc} (K)[c]	Φ (K)[d]	T_{max} (K)[e]	J_{exp} (K)[e]
TTT-NN	−23.9	−14.7	−25.7	10.0	−11.9
TPT-NN	−11.1	−5.3	−32.4	3.8	−6.2
PTP-NN	−2.7	*f*	*f*	*f*	*f*
PPP-NN	−2.1	−2.5	*f*	*f*	*f*

[a]The T_{max} denotes the position of the maximum in χ_{mol} (T), (cm^3/mol) as a function of temperature, and Φ (K) represents the Weiss temperature. [b]Calculated from an optimized structure using UBLYP/6-31G(d). [c]Calculated from an X-ray structure using UBLYP/6-31G(d). [d]Estimated from Curie−Weiss model. [e]Calculated from molar magnetic susceptibility, χ_{mol} (cm^{-1} mol^{-1}) as a function of temperature. [f]Not determined.

is mainly due to the different geometries from optimization versus X-ray structures differing mainly in the torsional angles between the radical unit NN and the π-bridge. Very interestingly, J_{calc} from the X-ray structure provided very close values to the ones obtained experimentally from magnetization measurements J_{exp} (Table 3) as found also in other cases before.[41,45]

The UBLYP functional and 6-31G(d) basis set are necessary since when calculating J values with the UB3LYP functional and 6-31G(d) basis set, it is well-known that the overestimation of $J_{intra}(calc)$ occurs due to the spin contamination from Hartree−Fock contributions.[60] This was also found here (Table S3). The theoretical exchange interaction of the **TTT-NN** was studied previously with the UB3LYP functional,[61] leading to stronger exchange than that with BLYP functional. From the triplet state, the spin density distributions were derived for **TPT-NN** and **TTT-NN**. The spin density is delocalized most on the O−N−C−N-O fragment of NN with a small spin density distribution into the connected thiophenes and a very minor spin found at the central phenyl ring in **TPT-NN** and the central thiophene unit in **TTT-NN** (Figure S17).

Magnetic Properties. The molar magnetic susceptibility (χ_{mol}) of the polycrystalline sample for **TTT-NN** and **TPT-NN** was recorded using a SQUID magnetometer in the temperature range 2 K ≤ T ≤ 300 K to elucidate magnetizations and magnetic exchange interaction as shown in Figure 8.

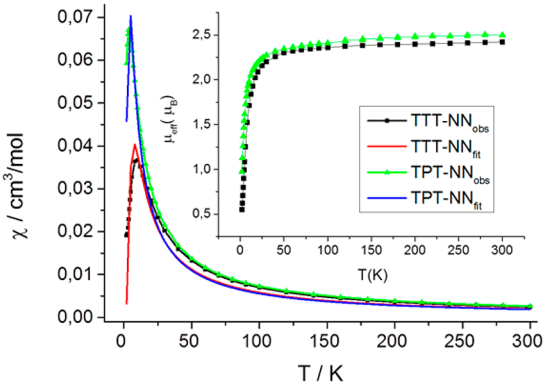

Figure 8. Molar magnetic susceptibility χ_{mol} (cm^3 mol^{-1}) of **TPT-NN** and **TTT-NN**. Inset: Effective magnetic moment, μ_{eff}, as a function of temperature.

The data reveal that both the samples behave almost temperature independent in the range from about 100 to 300 K. The molar magnetic susceptibility (χ_{mol}) initially increased by decreasing the temperature with the Curie−Weiss behavior at a higher temperature region (~150−10 K for **TTT-NN** and 150−3.8 K for **TPT-NN**) and decreased by decreasing the temperature at lower temperature (<10 ± 0.5 K for **TTT-NN** and <3.8 ± 0.5 K for **TPT-NN**) mainly caused by intramolecular antiferromagnetic (AF) interactions, which means that the biradicals switch from a thermally populated magnetic spin triplet state to a nonmagnetic spin singlet ground state.

The mean value for the magnetic exchange coupling at a high-temperature regime can be obtained by fitting the curve with inverse magnetic susceptibility $1/\chi_{mol}$ by a Curie−Weiss model straight line (Figure S18). The fitting negative Weiss temperatures are ΦW = −32.4 ± 0.5 K and −25.7 ± 0.5 K for **TTT-NN** and **TPT-NN**, respectively. These negative Weiss constants indicate that there is an intramolecular antiferromagnetic coupling interaction between NN radical units through the π-bridge. For a more precise determination of the intradimer, the coupling constant J_{intra} of **TTT-NN** and **TPT-NN** was estimated by the temperature dependence of the molar magnetic susceptibility over the temperature range 2 K ≥ T ≤ 300 K using the Bleaney−Bowers equation for isolated dimer models.[62] The intradimer magnetic exchange coupling constant J_{intra} between two $S = 1/2$ spins used in this expression refers to a Hamiltonian of the form $H = -2J_{12}S_1S_2$, which was taken also for the DFT calculations. These coupling constants are $J/k_B = -6.2$ K for **TPT-NN** and $J/k_B = -11.9$ K for **TTT-NN**, respectively. The observed effective magnetic moment (μ_{eff}) values for **TTT-NN** and **TPT-NN** are calculated from the temperature dependence of magnetic susceptibility as a function of temperature (inset of Figure 8).

At room temperature, the magnetic moments are close to the theoretical value 2.45 μB for magnetically uncorrelated spins of biradicals. The theoretical exchange coupling constants as J/k_B

DOI: 10.1021/acs.joc.7b00435
J. Org. Chem. 2017, 82, 7764−7773

calculated from optimized structure using UBLYP/6-31G(d) are listed in the Table 3. We did not further inspect the susceptibility experiment for **PPP-NN** and **PTP-NN** because the calculated coupling constant from DFT are very low as $J/k_B = -2.1$ K for **PPP-NN** and $J/k_B = -2.7$ K for **PTP-NN**, which are less interesting for the molecular quantum magnets.

CONCLUSIONS

In summary, we have designed and synthesized four nitronyl nitroxide biradicals with different numbers of phenyl and thiophene units as molecular bridges. The intramolecular magnetic interactions were predicted by the spin polarization rule, and the NN groups are AFM coupled to each other. All of the precursors were characterized by NMR spectroscopy and mass spectrometry, and **3**, **5**, **6**, **PPP-NNSi**, and **PTP-NNSi** were confirmed by single crystal X-ray studies. The structure of biradicals (**TPT-NN**, **TTT-NN**, and **PPP-NN**) were confirmed by single crystal X-ray studies, and their intra- and intermolecular packing were investigated. All of the biradicals were characterized by EPR spectroscopy and compared with computer simulation. Variable temperature and low temperature EPR studies as $\Delta M_S = 1$ and $\Delta M_S = 2$ were carried out. The biradicals were examined by UV−vis spectroscopy. The thiophene containing biradicals demonstrated more red-shifted absorption than the *p-ter*-phenyl based biradicals.

The strength of intramolecular magnetic interactions depends on the distance of the π-bridges and torsion between the aromatic rings in the π-bridge and between the π-bridge and the NN unit. The distance between the radical centers follows the trend **PPP-NN** > **PTP-NN** > **TPT-NN** > **TTT-NN**, and the order of the planarity of the π-bridges was PPP < PTP < TPT < TTT. The torsion of the thiophene and NN is smaller than that for the neighboring phenyl and NN units due to the smaller steric hindrance of five vs six membered rings. The calculated magnetic interactions for the optimized structures deviated more than those estimated from a single crystal X-ray structure with experimental values. These deviations due to optimized structures are more planar than the single crystal X-ray structures. The calculated magnetic interactions from the single crystal X-ray structure are quite similar to the experimental values for **TTT-NN** and **TPT-NN**. The biradicals (**TPT-NN** and **TTT-NN**) are promising molecules for further assessment because the magnetic coupling constants are −6.2 K for **TPT-NN** and −11.9 K for **TPT-NN**.

EXPERIMENTAL SECTION

Materials and Methods. Oven-dried glassware were used. All manipulations were performed under a dry argon atmosphere using a standard technique. NMR spectra were recorded using 250, 300, 500, or 700 MHz Bruker spectrometers. Chemical shifts are reported for ^{1}H NMR and ^{13}C NMR relative to residual proton or carbon resonances in CD_2Cl_2, DMSO-d_6, or THF-d_8. Molecular mass was recorded using ESI HRMS or MALDI-TOF mass spectrometric analyses. All reagents and chemicals were purchased from commercial sources and used as received, unless otherwise specified. The compounds 2,3-bis-(hydroxyamino)-2,3-dimethylbutane (BHA), **2**[63] and **4**,[64] were synthesized by modified reported procedures.

DFT Calculations. Geometry optimizations of the all of the structures were performed with full relaxation of all atoms in gas phase and without solvent effects carried out by the Gaussian 09 program using the B3LYP functional and 6-31G(d) basis set.[54]

UV−Vis and EPR Spectroscopy. UV−vis absorption spectra were recorded at room temperature using a PerkinElmer Lambda 900 spectrophotometer. The spectroscopic experiments were carried out in toluene as a solvent at room temperature. The EPR spectra were recorded in an argon-purged toluene as solvent ($\sim 10^{-4}$ M) on a Bruker EMX-plus spectrometer equipped with an NMR gauss meter and a variable-temperature control continuous-flow-N_2 cryostat (Bruker B-VT 2000).

X-ray Crystallography. The X-ray crystallographic data were collected on a Smart CCD diffractometer using a graphite monochromator Mo−Kα as a radiation source for **TPT-NN** at 23 °C and a STOE IPDS 2T diffractometer using a graphite monochromator Mo−Kα as a radiation source for **TTT-NN** at −100 °C and Cu−K_α IμS mirror system as a radiation source for **PPP-NN** at −153 °C. The structures were solved by direct methods (SIR-2004) and refined by SHELXL-2014 (full matrix), and 176 refined parameters for **TPT-NN**, 342 refined parameters for **TTT-NN**, and 186 refined parameters for **PPP-NN** were used. The X-ray crystallographic data and structure refinement information on **3**, **5**, **6**, **PPP-NNSi**, and **PTP-NNSi** are given in Table S1.

*2-(5-Bromothiophen-2-yl)-4,4,5,5-tetramethylimidazolidine-1,3-diol (**2**).* A mixture of 2,3-bis(hydroxylamino)-2,3-dimethylbutane (1.02 g, 6.75 mmol) and of 5-bromo-2-thiophenecarboxaldehyde (1.31 g, 6.75 mmol) in 10 mL of methanol was taken in a 50 mL round-bottomed flask, and the reaction mixture was stirred for 24 h at room temperature under argon atmosphere. The solution was filtered to obtain **2** as white powder (1.73 g, 80%). ^{1}H NMR (300 MHz, DMSO-d_6) δ: 1.02 (s, 6H), 1.04 (s, 6 H) 4.69 (s, 1 H), 6.9 (d, J = 3.9 Hz, 1H), 7.04 (d, J = 3.91 Hz, 1 H), 8.02 (s, 2 H). ^{13}C NMR (75 MHz, $CDCl_3$), δ: 17.2, 24.1, 66.4, 86.6, 110.6, 126.4, 129.5, 149.4. ESI HRMS calculated for $C_{11}H_{17}BrN_2O_2SNa$: 343.0092; found, 343.0090, $[M + Na]^+$.

*2-(5-Bromothiophen-2-yl)-1,3-bis((tert-butyldimethylsilyl)oxy)-4,4,5,5-tetramethylimidazolidine (**3**).* A DMF solution (10 mL) of **2** (1.01 g, 3.11 mmol), *t*-butyldimethylsilyl chloride (2.34 g, 5.56 mmol), and imidazole (2.14 g, 31.44 mmol) in a 50 mL Schlenk flask and the reaction mixture were stirred for 24 h at 50 °C under argon atmosphere. The solvent was removed under reduced pressure, then the crude product was extracted with ether and washed with water. The ether layer was dried over magnesium sulfate and concentrated under reduced pressure. The residue was chromatographed on silica gel with hexane as the eluant to give **3** (1.60 g, 93%). mp 69−70 °C. ^{1}H (300 MHz, CD_2Cl_2) δ: −0.52 (s, 6 H, $SiCH_3$), −0.04 (s, 6 H, $SiCH_3$), 0.83 (s, 18 H, Si-*t*-Bu), 1.13 (s, 12 H, CCH_3), 4.87 (s, 1 H, CH), 6.75 (d, 2 H, J = 4.0 Hz, Ar), 6.84 (d, 2 H, J = 4 Hz). ^{13}C NMR (75 MHz, $CDCl_3$) δ: −4.6, −3.7, 17.5, 18.5, 24.6, 26.6, 68.7, 90.6, 113.9, 128.7, 129.9, 149.2. ESI HRMS calculated for $C_{23}H_{46}BrN_2O_2SSi_2$: 549.2002; found, 549.2000, $[M + H]^+$.

TPT-NNSi. 1,4-Benzenediboronic acid bis(pinacol) ester, (0.15 g, 0.45 mmol), **3** (0.59 g, 1.08 mmol), K_2CO_3 (0.38 g, 2.71 mmol), and $Pd(PPh_3)_4$ (0.105 g, 0.09 mmol) were taken in a 50 mL Schlenk tube, and argon purged THF (15 mL) and water (3 mL) were added; then, the mixture was stirred for 24 h at 60 °C under argon atmosphere. The mixture was poured into water and extracted with ether. The ether layer was dried over magnesium sulfate, and the solution was concentrated under reduced pressure. The residue was chromatographed on silica gel with hexane as eluant to obtain **TPT-NNSi** (0.37 g, 81%). mp 236−237 °C. ^{1}H NMR (300 MHz, CD_2Cl_2) δ: −0.51 (s, 12 H, $SiCH_3$), −0.05 (s, 12 H, $SiCH_3$), 0.83 (s, 36 H, Si-*t*-Bu), 1.16 (s, 24 H, CCH_3), 4.92 (s, 2 H, CH), 6.96 (d, 2 H, J = 4 Hz, Ar), 7.15 (d, 2 H, J = 4 Hz), 7.62 (s, 4 H). ^{13}C NMR (175 MHz; $CDCl_3$) δ: − 4.8, −3.7, 17.6, 18.5, 25.2, 26.6, 30.3, 68.7, 91.0, 121.9, 126.3, 130.6, 134.4, 145.4, 147.4. ESI HRMS calculated for $C_{52}H_{95}N_4O_4S2Si_4$: 1015.5872; found, 1015.5897, $[M + H]^+$.

TPT-NN. A precursor **TPT-NNSi** (0.20 g, 0.21 mmol) was dissolved in dry THF (15 mL) in a round-bottomed flask, and (4.7 mL) Bu_4NF and 1 M solution in THF were added; then, the mixture was stirred for 16 h at room temperature while the reaction was monitored by TLC. The product was concentrated under reduced pressure, and the mixture was purified by column chromatography with DCM and MeOH (0−2%) as eluant to provide **TPT-NN** as a green solid (90 mg, 83%). mp, decompd. 245−246 °C. ESI HRMS calculated for $C_{28}H_{32}N_4O_4NaS_2$: 575.1763; found, 575.1759 $[M + Na]^+$.

DOI: 10.1021/acs.joc.7b00435
J. Org. Chem. 2017, 82, 7764−7773

*2-(4-Bromophenyl)-4,4,5,5-tetramethylimidazolidine-1,3-diol, (**4**).* A mixture of 2,3-bis(hydroxylamino)-2,3-dimethylbutane (2.9 g, 19.6 mmol) and of 4-bromobenzaldehyde (3.6 g, 19.6 mmol) in 30 mL of methanol in a 50 mL round-bottomed flask was stirred for 24 h at room temperature under argon atmosphere. The solution was filtered to obtain **4** as a white powder (5.3 g, 86%). ^{1}H NMR (300 MHz, DMSO-d_6) δ: 1.03 (s, 6 H, CH_3), 1.06 (s, 6 H, CH_3), 4.47 (s, 1 H, CH), 7.41 (d, 2 H, J = 9.0 Hz, Ar), 7.50 (d, 2 H, J = 8.0 Hz, Ar), 7.81 (s, 2 H, OH). ^{13}C NMR (75 MHz, DMSO-d_6) δ: 17.2, 24.4, 66.2, 89.6, 120.4, 130.5, 130.6, 141.4. ESI HRMS calculated for $C_{13}H_{20}BrN_2O_2$: 315.0703; found, 315.0694 $[M + H]^+$.

*2-(4-Bromophenyl)-1,3-bis((tert-butyldimethylsilyl)oxy)-4,4,5,5-tetramethylimidazolidine, (**5**).* The 2-(4-Bromophenyl)-4,4,5,5-tetramethylimidazolidine-1,3-diol, **4** (3.0 g, 9.5 mmol), *t*-butyldimethylsilyl chloride (7.2 g, 47.6 mmol), and imidazole (6.5 g, 95.2 mmol) were dissolved in dry DMF (45 mL) in a 100 mL Schlenk flask, and the mixture was stirred for 24 h at 50 °C under argon atmosphere. DMF was removed under reduced pressure and extracted with diethyl ether and washed with water. The organic layer was dried over magnesium sulfate and concentrated under reduced pressure. The residue was purified by column chromatography on silica gel with hexane as the eluant to give **5** as a white powder (4.8 g, 92%). ^{1}H NMR (300 MHz, CD_2Cl_2) δ: −0.84 (s, 6 H, $SiCH_3$), −0.04 (s, 6 H, $SiCH_3$), 0.79 (s, 18 H, Si-*t*-Bu), 1.16 (s, 12 H, CCH_3), 4.59 (s, 1 H, CH), 7.26 (d, 2 H, J = 10 Hz, Ar), 7.40 (d, 2 H, J = 10 Hz). ^{13}C NMR (125 MHz, CD_2Cl_2) δ: −19.1, −17.6, − 3.2, −3.9, 10.52, 12.1, 54.2, 79.5, 107.8, 116.7, 118.8. ESI HRMS calculated for $C_{25}H_{48}BrN_2O_2Si_2$: 543.2438; found, 543.2419, $[M + H]^+$.

PPP-NNSi. A mixture of 1,4-benzenediboronic acid bis(pinacol) ester, (0.15 g, 0.45 mmol), 2-(4-bromophenyl)-1,3-bis((*tert*-butyldimethylsilyl)oxy)-4,4,5,5-tetramethylimidazolidine, **5** (0.50 g, 0.91 mmol), K_2CO_3 (0.19 g, 1.38 mmol), and $Pd(PPh_3)_4$ (0.05 g, 0.09 mmol) was taken in a 50 mL Schlenk tube, and argon purged THF (20 mL) and water (5 mL) were added. Then, the mixture was stirred for 24 h at 60 °C under argon atmosphere. The mixture was poured into water and filtered to give **PPP-NNSi** as a white solid (0.34 g, 74%). mp 248−249 °C. ^{1}H NMR (300 MHz, CD_2Cl_2) δ: −0.77 (s, 12 H, $SiCH_3$), −0.02 (s, 12 H, $SiCH_3$), 0.82 (s, 36 H, Si-*t*-Bu), 1.22 (s, 24 H, CCH_3), 4.71 (s, 1 H, CH), 7.49 (d, 2 H, J = 10 Hz, Ar), 7.65 (d, 2 H, J = 10 Hz), 7.71 (s, 4 H). ^{13}C NMR (125 MHz, CD_2Cl_3) δ: −4.5, −3.3, 17.8, 18.8, 25.9, 26.9, 30.7, 69.3, 95.0, 126.9, 128.0, 132.2, 140.7, 141.6. ESI HRMS calculated for $C_{56}H_{99}N_4O_4Si_4$: 1003.6743; found, 1003.6768, $[M + H]^+$.

PPP-NN. **PPP-NNSi** (0.10 g, 0.10 mmol) was dissolved in dry THF (10 mL) and (2.4 mL,) and 1 M solution of Bu_4NF in THF was added; then, the mixture was stirred for 3 h at room temperature, while the reaction was monitored by TLC. The reaction mixture was concentrated under reduced pressure, and then, the crude product was purified by column chromatography, DCM, and MeOH (0−2%) as eluant to obtain **PPP-NN** as a blue solid (0.037 g, 68%). mp, decompd. 260−261 °C. ESI HRMS calculated for $C_{32}H_{36}N_4O_4Na$: 563.2634; found, 563.2650, $[M + Na]^+$.

*1,3-Bis((tert-butyldimethylsilyl)oxy)-4,4,5,5-tetramethyl-2-(4-(4,4,5,5-tetramethyl-1,3,2-dioxaborolan-2-yl)phenyl)imidazolidine (**6**).* Compound **5** (4.80 g, 8.83 mmol) was dissolved in dry THF (50 mL) in a 100 mL Schlenk tube and cooled to −78 °C; then, *n*-butyllithium (1.6 M solution) in hexane (6.7 mL, 10.56 mmol) was added, and the mixture was stirred at the same temperature for 1 h. Then, 2-isopropylboronic acid and pinacol ester (1.97 g, 2.16 mL, 10.59 mmol) was added, and the reaction mixture was stirred at the same temperature for a further 1 h, then quenched with water (10 mL) and extracted with ether. The ether layer was dried over magnesium sulfate and concentrated under reduced pressure. The residue was chromatographed on silica gel with hexane as eluant to obtain **6** (4.9 g, 94%). mp 132−133 °C. ^{1}H NMR (300 MHz, CD_2Cl_2) δ: −0.90 (s, 6 H, $SiCH_3$), −0.04 (s, 6 H, $SiCH_3$), 0.79 (s, 18 H, *t*-Bu), 1.17 (s, 12 H, CCH_3), 4.62 (s, 1 H, CH), 7.39 (d, 2 H, J = 6 Hz), 7.65 (d, 2 H, J = 9 Hz). ^{13}C NMR (125 MHz; CD_2Cl_2) δ; −4.7, −3.5, 17.7, 18.4, 25.1, 25.4, 26.6, 68.7, 84.3, 94.9, 129.2, 130.9, 134.5, 145.2. ESI HRMS calculated for $C_{31}H_{60}BN_2O_4Si_2$: 590.4215; found, 590.4205 $[M + H]^+$.

PTP-NNSi. 2,5-Dibromothiophene, (0.10 g, 0.42 mmol), **6** (0.50 g, 0.85 mmol), K_2CO_3 (0.35 g, 2.53 mmol), and $Pd(PPh_3)_4$ (0.11 g, 0.09 mmol) were taken in a 50 mL Schlenk tube, and then argon purged THF (15 mL) and water (5 mL) were added. The mixture was stirred for 24 h at 60 °C under argon atmosphere. Then, the mixture was poured into water and extracted with ether. The ether layer was dried over magnesium sulfate and concentrated under reduced pressure. The residue was chromatographed on silica gel with hexane to obtain **PTP-NNSi** (0.28 g, 66%). mp 210−211 °C. ^{1}H NMR (250 MHz, CD_2Cl_2) δ: −0.78 (s, 12 H, $SiCH_3$), −0.01 (s, 12 H, $SiCH_3$), 0.81 (s, 36 H, Si-*t*-Bu), 1.19 (s, 24 H, CCH_3), 4.65 (s, 1 H, CH), 7.35 (s, 2 H), 7.42 (d, 2 H, J = 7.5 Hz), 7.60 (d, 4 H, J = 7.5 Hz). ^{13}C NMR (125 MHz; CD_2Cl_3) δ: −4.6, −3.5, 17.6, 18.4, 25.1, 26.6, 68.6, 94.1, 124.3, 125.1, 132.1, 134.3, 141.7, 143.9. ESI HRMS calculated for $C_{54}H_{97}N_4O_4Si_4S$: 1009.6308; found 1009.6298 $[M + H]^+$.

PTP-NN. **PTP-NNSi** (0.05 g, 0.05 mmol) was dissolved in dry THF (1.19 mL) and Bu_4NF. 1 M solution in THF was added, then the mixture was stirred for 16 h at room temperature, while the reaction was monitored by TLC. The reaction mixture was concentrated under reduced pressure, and the mixture was purified by column chromatography, DCM, and MeOH (0−2%) as eluant to obtain **PTP-NN** (18 mg, 70%). mp, decompd. mp 206−207 °C. MALDI-TOF calculated for $C_{30}H_{34}N_4O_4S$; 546.6900; found, 546.2100 $[M]^+$.

TTT-NNSi. Thiophene-2,5-diboronic acid bis(pinacol) ester (0.20 g, 0.59 mmol), **3** (0.72 g, 1.31 mmol), K_2CO_3 (0.49 g, 3.57 mmol), and $Pd(PPh_3)_4$ (0.07 g, 0.06 mmol) were taken in a Schlenk tube, and argon purged THF (30 mL) and water (10 mL) were added. Then, the mixture was stirred for 24 h at 60 °C under argon atmosphere. The mixture was poured into water and extracted with diethyl ether. The ether layer was dried over magnesium sulfate and concentrated under reduced pressure. The residues were chromatographed on silica gel with hexane as an eluent to obtain TTT-NNSi (0.11 g, 18%). ^{1}H NMR (300 MHz, CD_2Cl_2) δ: −0.51 (s, 12 H, $SiCH_3$), −0.05 (s, 12 H, $SiCH_3$), 0.83 (s, 36 H, Si-*t*-Bu), 1.16 (s, 24 H, CCH_3), 4.92 (s, 1 H, CH), 6.96 (d, 2 H, J = 4 Hz, Ar), 7.15 (d, 2 H, J = 4 Hz), 7.62 (s, 4 H). ^{13}C NMR (125 MHz, $CDCl_3$) δ: −4.7, −3.7, 17.5, 18.5, 25.1, 26.5, 30.3, 68.7, 122.4, 124.3, 130.1, 137.1, 138.7, 146.9. ESI HRMS calculated for $C_{50}H_{93}N_4O_4S_3Si_4$: 1021.5436; found 1021.5461, $[M + H]^+$. Monocoupled product: 0.171 g, 51%. ^{1}H NMR (300 MHz, CD_2Cl_2) δ: −0.51 (s, 12 H, $SiCH_3$), −0.05 (s, 12 H, $SiCH_3$), 0.83 (s, 36 H, Si-*t*-Bu), 1.16 (s, 24 H, CCH_3), 4.92 (s, 1 H, CH), 6.96 (d, 2 H, J = 4 Hz, Ar), 7.15 (d, 2 H, J = 4 Hz), 7.62 (s, 4 H).

TTT-NNSi. By Stille coupling, 2,5-bis(trimethylstannyl)thiophene (0.10 g, 0.23 mmol), **3** (0.33 g, 0.61 mmol), and $Pd(PPh_3)_4$ (0.06 g, 0.05 mmol) were taken in a 50 mL Schleck tube, and argon purged dry DMF (10 mL) was added, then the mixture was stirred for 30 h at 60 °C. Then, DMF was removed under reduced pressure. The residue was extracted with diethyl ether (2 × 50 mL). The ether layer was dried over magnesium sulfate and concentrated under reduced pressure. The residue was chromatographed on silica gel with hexane to obtain **TTT-NNSi** (0.18 g, 79%).

TTT-NN. **TTT-NNSi** (0.10 mg, 0.10 mmol) was dissolved in dry THF (7 mL) and (2.4 mL) Bu_4NF, and 1 M solution in THF was added. Then, the mixture was stirred for 16 h at room temperature, while the reaction was monitored by TLC. The solution was concentrated under reduced pressure, and the mixture was purified by column chromatography, DCM, and MeOH (0−2%) as eluant to obtain **TTT-NN** as a green solid (36 mg, 66%). mp, decompd. 219−220 °C. ESI calculated for $C_{26}H_{30}N_4O_4S_3$: 558.14; found, 558.16 $[M]^+$.

■ ASSOCIATED CONTENT

Supporting Information

The Supporting Information is available free of charge on the ACS Publications website at DOI: 10.1021/acs.joc.7b00435.

Optimized structure of π bridges, prediction of magnetic interaction, and structures and refinement details of **3**, **5**, **6**, **PPP-NNSi**, and **PTP-NNSi**, and structures of the **TPT-NN**, **TTT-NN**, and **PPP-NN**, optical spectra and

DOI: 10.1021/acs.joc.7b00435
J. Org. Chem. 2017, 82, 7764−7773

optical data of **PPP-NNSi**, **PPP-NN**, **TPT-NNSi**, **TPT-NN**, **TTT-NNSi**, **TTT-NN**, and **PTP-NNSi**, **PPP-NN** in dilute toluene, EPR spectra of the biradicals in toluene, EPR spectra of **T-NN**, monoradical, and **TTT-NN** in toluene, optimized structures of **PPP-NN**, **TTT-NN**, **TPT-NN**, and **PTP-NN**, the magnetic exchange coupling calculated J_{calc} by optimized structure using U3BLYP/6-31G(d), and X-ray structure using U3BLYP/6-31G, calculated spin density distribution of the triplet state of **TPT-NN** and **TTT-NN**, Curie−Weiss model straight line of **TPP-NN** and **TTT-NN**, characterization of new compounds, NMR spectra, and DFT calculations data and reference (PDF)

Crystallographic data for compounds **3**, **5**, **6**, **PPP-NNSi**, and **PTP-NNSi**, **TPT-NN**, **TTT-NN**, and **PPP-NN** (CIF)

AUTHOR INFORMATION

Corresponding Author

*E-mail: martin.baumgarten@mpip-mainz.mpg.de.

ORCID

Artem S. Bogomyakov: 0000-0002-6918-5459

Martin Baumgarten: 0000-0002-9564-4559

Present Address

[‖]P.R.: Department of Chemistry, University of Basel, St. Johanns-Ring 19, 4056 Basel, Switzerland.

Notes

The authors declare no competing financial interest.

ACKNOWLEDGMENTS

We acknowledge the SFB-TR49 for financial support.

REFERENCES

(1) Forrest, S. R. *Nature* **2004**, *428*, 911−918.
(2) Sokolov, A. N.; Roberts, M. E.; Bao, Z. *Mater. Today* **2009**, *12*, 12−20.
(3) Brabec, J.; Sariciftci, N. S.; Hummelen, J. C. *Adv. Funct. Mater.* **2001**, *11*, 15−26.
(4) Abe, M. *Chem. Rev.* **2013**, *113*, 7011−7088.
(5) Sorai, M.; Nakazawa, Y.; Nakano, M.; Miyazaki, Y. *Chem. Rev.* **2013**, *113*, PR41−PR122.
(6) Ratera, I.; Veciana, J. *Chem. Soc. Rev.* **2012**, *41*, 303−349.
(7) Sugawara, T.; Komatsu, H.; Suzuki, K. *Chem. Soc. Rev.* **2011**, *40*, 3105−3118.
(8) Coronado, E.; Day, P. *Chem. Rev.* **2004**, *104*, 5419−5448.
(9) Dunbar, K. R. *Inorg. Chem.* **2012**, *51*, 12055−12058.
(10) Blundell, S. J.; Pratt, F. L. *J. Phys.: Condens. Matter* **2004**, *16*, R771−R828.
(11) Das, K.; Pink, M.; Rajca, S.; Rajca, A. *J. Am. Chem. Soc.* **2006**, *128*, 5334−5335.
(12) Wang, J.; He, C.; Wu, P.; Wang, J.; Duan, C. *J. Am. Chem. Soc.* **2011**, *133*, 12402−12405.
(13) Itkis, M. E.; Chi, X.; Cordes, A. W.; Haddon, R. C. *Science* **2002**, *296*, 1443−1445.
(14) Jasiński, M.; Szczytko, J.; Pociecha, D.; Monobe, H.; Kaszyński, P. *J. Am. Chem. Soc.* **2016**, *138*, 9421−9424.
(15) Ravat, P.; Marszalek, T.; Pisula, W.; Mullen, K.; Baumgarten, M. *J. Am. Chem. Soc.* **2014**, *136*, 12860−12863.
(16) Rajca, A.; Wang, Y.; Boska, M.; Paletta, J. T.; Olankitwanit, A.; Swanson, M. A.; Mitchell, D. G.; Eaton, S. S.; Eaton, G. R.; Rajca, S. *J. Am. Chem. Soc.* **2012**, *134*, 15724−15727.
(17) Sowers, M. A.; McCombs, J. R.; Wang, Y.; Paletta, J. T.; Morton, S. W.; Dreaden, E. C.; Boska, M. D.; Ottaviani, M. F.; Hammond, P. T.; Rajca, A.; Johnson, J. A. *Nat. Commun.* **2014**, *5*, 5460.
(18) Hayes, R. T.; Walsh, C. J.; Wasielewski, M. R. *J. Phys. Chem. A* **2004**, *108*, 2375−2381.
(19) Teki, Y.; Miyamoto, S.; Iimura, K.; Nakatsuji, M.; Miura, Y. *J. Am. Chem. Soc.* **2000**, *122*, 984−985.
(20) Aoki, K.; Akutsu, H.; Yamada, J.-i.; Nakatsuji, S.; rsquo; ichi; Kojima, T.; Yamashita, Y. *Chem. Lett.* **2009**, *38*, 112−113.
(21) Wang, Y.; Wang, H.; Liu, Y.; Di, C.-a.; Sun, Y.; Wu, W.; Yu, G.; Zhang, D.; Zhu, D. *J. Am. Chem. Soc.* **2006**, *128*, 13058−13059.
(22) Nakatsuji, S.; rsquo; ichi; Aoki, K.; Akutsu, H.; Yamada, J.-i.; Kojima, T.; Nishida, J.-i.; Yamashita, Y. *Bull. Chem. Soc. Jpn.* **2010**, *83*, 1079−1085.
(23) Zhang, Y.; Basel, T. P.; Gautam, B. R.; Yang, X.; Mascaro, D. J.; Liu, F.; Vardeny, Z. V. *Nat. Commun.* **2012**, *3*, 1043.
(24) Kato, F.; Kikuchi, A.; Okuyama, T.; Oyaizu, K.; Nishide, H. *Angew. Chem., Int. Ed.* **2012**, *51*, 10177−10180.
(25) Yang, W.; Soderberg, M.; Eriksson, A. I. K.; Boschloo, G. *RSC Adv.* **2015**, *5*, 26706−26709.
(26) Yang, W.; Vlachopoulos, N.; Hao, Y.; Hagfeldt, A.; Boschloo, G. *Phys. Chem. Chem. Phys.* **2015**, *17*, 15868−15875.
(27) Nam, H.; Kwon, J. E.; Choi, M.-W.; Seo, J.; Shin, S.; Kim, S.; Park, S. Y. *ACS Sensors* **2016**, *1*, 392−398.
(28) Janoschka, T.; Hager, M. D.; Schubert, U. S. *Adv. Mater.* **2012**, *24*, 6397−6409.
(29) Tomlinson, E. P.; Hay, M. E.; Boudouris, B. W. *Macromolecules* **2014**, *47*, 6145−6158.
(30) Koivisto, B. D.; Hicks, R. G. *Coord. Chem. Rev.* **2005**, *249*, 2612−2630.
(31) Matuschek, D.; Eusterwiemann, S.; Stegemann, L.; Doerenkamp, C.; Wibbeling, B.; Daniliuc, C. G.; Doltsinis, N. L.; Strassert, C. A.; Eckert, H.; Studer, A. *Chem. Sci.* **2015**, *6*, 4712−4716.
(32) Train, C.; Norel, L.; Baumgarten, M. *Coord. Chem. Rev.* **2009**, *253*, 2342−2351.
(33) Onal, E.; Yerli, Y.; Cosut, B.; Pilet, G.; Ahsen, V.; Luneau, D.; Hirel, C. *New J. Chem.* **2014**, *38*, 4440−4447.
(34) Reis, S. G.; Briganti, M.; Martins, D. O. T. A.; Akpinar, H.; Calancea, S.; Guedes, G. P.; Soriano, S.; Andruh, M.; Cassaro, R. A. A.; Lahti, P. M.; Totti, F.; Vaz, M. G. F. *Dalton Trans.* **2016**, *45*, 2936−2944.
(35) Akita, T.; Mazaki, Y.; Kobayashi, K.; Koga, N.; Iwamura, H. *J. Org. Chem.* **1995**, *60*, 2092−2098.
(36) Zheludev, A.; Bonnet, M.; Delley, B.; Grand, A.; Luneau, D.; Örström, L.; Ressouche, E.; Rey, P.; Schweizer, J. *J. Magn. Magn. Mater.* **1995**, *145*, 293−305.
(37) Ravat, P.; Teki, Y.; Ito, Y.; Gorelik, E.; Baumgarten, M. *Chem. - Eur. J.* **2014**, *20*, 12041−1245.
(38) Ravat, P.; Baumgarten, M. *J. Phys. Chem. B* **2015**, *119*, 13649−13655.
(39) Osiecki, J. H.; Ullman, E. F. *J. Am. Chem. Soc.* **1968**, *90*, 1078−1079.
(40) Caneschi, A.; Gatteschi, D.; Sessoli, R.; Rey, P. *Acc. Chem. Res.* **1989**, *22*, 392−398.
(41) Borozdina, Y. B.; Mostovich, E.; Enkelmann, V.; Wolf, B.; Cong, P. T.; Tutsch, U.; Lang, M.; Baumgarten, M. *J. Mater. Chem. C* **2014**, *2*, 6618−6629.
(42) Mostovich, E. A.; Borozdina, Y.; Enkelmann, V.; Remović-Langer, K.; Wolf, B.; Lang, M.; Baumgarten, M. *Cryst. Growth Des.* **2012**, *12*, 54−59.
(43) Zoppellaro, G.; Ivanova, A.; Enkelmann, V.; Geies, A.; Baumgarten, M. *Polyhedron* **2003**, *22*, 2099−2110.
(44) Ravat, P.; Ito, Y.; Gorelik, E.; Enkelmann, V.; Baumgarten, M. *Org. Lett.* **2013**, *15*, 4280.
(45) Ravat, P.; Borozdina, Y.; Ito, Y.; Enkelmann, V.; Baumgarten, M. *Cryst. Growth Des.* **2014**, *14*, 5840−5846.
(46) Sachdev, S. *Nat. Phys.* **2008**, *4*, 173−185.
(47) Giamarchi, T.; Ruegg, C.; Tchernyshyov, O. *Nat. Phys.* **2008**, *4*, 198−204.
(48) Rüegg, C.; Kiefer, K.; Thielemann, B.; McMorrow, D. F.; Zapf, V.; Normand, B.; Zvonarev, M. B.; Bouillot, P.; Kollath, C.; Giamarchi,

DOI: 10.1021/acs.joc.7b00435
J. Org. Chem. 2017, 82, 7764−7773

T.; Capponi, S.; Poilblanc, D.; Biner, D.; Krämer, K. W. *Phys. Rev. Lett.* **2008**, *101*, 247202.
(49) Tutsch, U.; Wolf, B.; Wessel, S.; Postulka, L.; Tsui, Y.; Jeschke, H. O.; Opahle, I.; Saha-Dasgupta, T.; Valentí, R.; Brühl, A.; Remović-Langer, K.; Kretz, T.; Lerner, H. W.; Wagner, M.; Lang, M. *Nat. Commun.* **2014**, *5*, 5169.
(50) Tretyakov, E.; Okada, K.; Suzuki, S.; Baumgarten, M.; Romanenko, G.; Bogomyakov, A.; Ovcharenko, V. *J. Phys. Org. Chem.* **2016**, *29*, 725−734.
(51) Mitsumori, T.; Inoue, K.; Koga, N.; Iwamura, H. *J. Am. Chem. Soc.* **1995**, *117*, 2467−2478.
(52) Higashiguchi, K.; Yumoto, K.; Matsuda, K. *Org. Lett.* **2010**, *12*, 5284−5286.
(53) Yokojima, S.; Kobayashi, T.; Shinoda, K.; Matsuda, K.; Higashiguchi, K.; Nakamura, S. *J. Phys. Chem. B* **2011**, *115*, 5685−5692.
(54) Frisch, M. J.; Trucks, G. W.; Schlegel, H. B.; Scuseria, G. E.; Robb, M. A.; Cheeseman, J. R.; Scalmani, G.; Barone, V.; Mennucci, B.; Petersson, G. A., et al. *Gaussian 09*, revision D.01; Gaussian Inc.: Wallingford, CT, 2013.
(55) Noodleman, L. *J. Chem. Phys.* **1981**, *74*, 5737−5743.
(56) Noodleman, L.; Davidson, E. R. *Chem. Phys.* **1986**, *109*, 131−143.
(57) Yamaguchi, K.; Jensen, F.; Dorigo, A.; Houk, K. N. *Chem. Phys. Lett.* **1988**, *149*, 537−542.
(58) Soda, T.; Kitagawa, Y.; Onishi, T.; Takano, Y.; Shigeta, Y.; Nagao, H.; Yoshioka, Y.; Yamaguchi, K. *Chem. Phys. Lett.* **2000**, *319*, 223−230.
(59) Shoji, M.; Koizumi, K.; Kitagawa, Y.; Kawakami, T.; Yamanaka, S.; Okumura, M.; Yamaguchi, K. *Chem. Phys. Lett.* **2006**, *432*, 343−347.
(60) Plakhutin, B. N.; Gorelik, E. V.; Breslavskaya, N. N.; Milov, M. A.; Fokeyev, A. A.; Novikov, A. V.; Prokhorov, T. E.; Polygalova, N. E.; Dolin, S. P.; Trakhtenberg, L. I. *J. Struct. Chem.* **2005**, *46*, 195−203.
(61) Nishizawa, S.; Hasegawa, J.-y.; Matsuda, K. *J. Phys. Chem. C* **2015**, *119*, 5117−5121.
(62) Bleaney, B.; Bowers, K. D. *Proc. R. Soc. London, Ser. A* **1952**, *214*, 451−465.
(63) Kirk, M. L.; Shultz, D. A.; Stasiw, D. E.; Lewis, G. F.; Wang, G.; Brannen, C. L.; Sommer, R. D.; Boyle, P. D. *J. Am. Chem. Soc.* **2013**, *135*, 17144−17154.
(64) Wautelet, P.; Le Moigne, J.; Videva, V.; Turek, P. *J. Org. Chem.* **2003**, *68*, 8025−8036.

DOI: 10.1021/acs.joc.7b00435
J. Org. Chem. 2017, 82, 7764−7773